KINETICS AND MECHANISMS OF NANOCRYSTALLINE MGFE$_2$O$_4$/ CUFE$_2$O$_4$ CORE/SHELL REDUCTION IN FLOWING HYDROGEN AT 400–700 ^{O}C

M. Bahgat[a], M. H. Khedr[b], and W.M.A.El Rouby[c]

ABSTRACT:

Copper ferrite nanoparticles are coated with magnesium ferrite nanoparticles to form CuFe$_2$O$_4$/ MgFe$_2$O$_4$ core/shell structure by hydrothermal precipitation method. The final precipitate was filtered, washed thoroughly with deionized water and dried at 343K for 24 h. The resulting sample was then calcined at 1173K for 2 h giving the magnetic material CuFe$_2$O$_4$/MgFe$_2$O$_4$ core/shell. The fired powder is then pressed in form of pellets and sintered at 500 ^{o}C for 2 h. CuFe$_2$O$_4$/ MgFe$_2$O$_4$ core/shell were isothermally reduced in hydrogen flow at 400-700 ^{o}C. The reduced nano-crystalline CuFe$_2$O$_4$/MgFe$_2$O$_4$ core/ shell compacts were characterized by XRD, TEM, SEM, VSM and reflected light microscope. Microstructure of partially and completely reduced samples was studied and the activation energy values were calculated from Arrhenius equation. The activation energy of the initial stage was found to be 9.2kJ/mol, and for the final stage is found to be 23kJ/mol. The approved mathematical formulations for the gas solid reaction were applied and it was found that at the initial stages the reaction is controlled by gaseous diffusion mechanism while the final reaction stages is controlled by the combined gaseous diffusion and interfacial chemical reaction mechanisms.

KEYWORDS:

Core–shell, Nanoparticles, Reduction, kinetics, mechanisms and magnetic properties.

---

[a] Researcher, Central Metallurgical Research and Development Institute (CMRDI), Helwan, Egypt.
[b] Prof. of Materials Science , Chemistry Department, Faculty of Science, Beni-Sueif University, Beni-Sueif, Egypt.

[c] Faculty of Science, Beni-Sueif University, Beni-Sueif, Egypt

1-INTRODUCTION:

The fast developments in science and technology need materials with specific properties to satisfy the requirement of the area of application. Nanocrystalline materials are showing great promise in industry and technology [1]. This is mainly because they have some unique properties which are not showed by the bulk crystalline materials [2, 3]. The synthesis of ultra fine magnetic powders for applications such as magnetic recording and magnetic fluids has received wide attention in recent years [4, 5]. A nanocomposite is a material that contains a reinforcement component in the form of one or more ultrafine phase with dimensions less than 100 nm. The nanocomposite approach has been used to improve various material properties including mechanical, chemical, structural, optical, and electrical/magnetic properties [6]

The preparation of metallic nanoparticles attracts considerable interests because of their unique physical and chemical properties [7–9]. Surface coating of nanoparticles with various materials forming core–shell morphologies results in the formation of materials that can be used for development of catalysts and optoelectronic devices [10]. The core–shell structures have also been used as precursors to prepare hollow structures by the complete removal of core materials through chemical etching or combustion, and partial elimination of the core have enabled preparation of novel nanostructures inside the shell [11–13]. In a core/shell nanomaterial both the chemical composition and size of core and shell can be tailored to obtain required properties. Nanotechnology concerns itself with the ability to manipulate fully the properties of nanostructured materials, via their size, shape and composition [14–16], and also to develop reproducible, complex structures from simpler systems [17–19]. This can apply to magnetic nanoparticle systems, in which the nanoparticles often need to be incorporated into more complex structures to allow specific properties to be harnessed, or to adapt the particles for a specific application or environment. Synthesis of metal nanoparticles has been achieved by a variety of different methods including colloid chemistry [20], cluster source deposition [21] and even mechanical milling [22]. Also, with a high surface activity owing to their small particle size and enormous surface area, it has been used for various applications including recording media, microwave absorbents and sensors.

Therefore, recently, the reduction of ferrites has attracted increasing attention as an interesting chemical treatment potential for the preparation of nano sized magnetic based materials with improved magnetic properties. On the other hand, reduction of ferrites is an important step in metallurgical processes as applied to M–Fe–O systems and also in developing master alloys in steel production, in spite of that it is not covered well through the research investigations.

The mechanism and kinetics of reduction of different ferrites such as ferrites of cobalt, zinc and strontium were investigated.[23–26]. Khedr et.al [27] studied the kinetics and mechanisms of nano-crystalline $CuFe_2O_4$ reduction in hydrogen at 300-600 ^{o}C found that the reduction of copper ferrite is not completed at 300 ^{o}C but goes to completion (100%) at 400-600 ^{o}C leading to the formation of metallic nano-wires of

iron (106nm) and copper (56nm). Bahgat et.al [28] studied kinetics and mechanisms of reduction of nano-crystalline $MgFe_2O_4$ in pure hydrogen at 800-1000 ^oC that leads to the formation of Fe/MgO nanocomposite (77nm). He found that the magnetic properties of the produced Fe/MgO nanocomposite enhanced as soft magnetic materials with increasing reaction temperature, whereas the Hc values decreased while the Ms and Mr values increased.

In this work we studied the kinetics and mechanisms of reduction of nano-crystalline $CuFe_2O_4/MgFe_2O_4$ core/shell in hydrogen at 400-700 ^oC were investigated. Magnetic properties of the reduced core/shell nanoparticles are studied. The structure of the reduced core/shell materials was studied using X-ray diffraction, TEM, SEM and light microscope.

2-EXPREMENTAL:

For synthesis of $CuFe_2O_4$, two moles of fine powder ferric acetate basic $(CH_3OO)_2Fe.OH$, are well mixed in ball mill for 6h with one mole of copper (II) acetate monohydrate $(CH_3OO)_2Cu.H_2O$ to ensure the homogeneity. The mixture is dried at 150 ^oC and the sample is heated on a hot plate to help decomposition of acetates and then fired for 2h at 600 ^oC to obtain the fine powder form. The fired sample is milled in a ball milling for 40 h to obtain small nanoparticles. Finally the powder heated in muffle furnace up to 1000 ^oC for 2h and then left to cool gradually[29]. $MgFe_2O_4$ nanoparticles were prepared by following the method described previously [30, 31].

$CuFe_2O_4/MgFe_2O_4$ core/shell was prepared by the same method. A mixed aqueous solution of $Mg(NO_3)_2.6H_2O$(10.723g/250ml), $Fe(NO_3)_3.9H_2O$ (33.91g/250 ml) and $CuFe_2O_4$ (10g/250ml) in deionized water and a second solution containing NaOH ($[NaOH]$ = 1.6 $[Mg^{2+}+Fe^{3+}]$) and Na_2CO_3 ($[CO_3^{2-}]$ = 2.0$[Fe^{3+}]$) in deionized water (pH~9) were simultaneously added to a colloid mill and mixed for 2 min. The resulting slurry was removed from the reactor into a three-neck flask and aged at 373K for 6 h. The final precipitate was filtered, washed thoroughly with deionized water and dried at 343K for 24 h. The resulting sample was then calcined at 1173K for 2 h giving the magnetic material, denoted as $CuFe_2O_4/MgFe_2O_4$ core/shell. The obtained powder is moistened with 10% water then compacts, with weights of 1.5 g, were prepared by pressing in cylindrical mould of 1 cm inner diameter at 200 kg/cm^2. The produced compact were left overnight then dried at 100 ^oC for 24 h. The dry compacts were then gradually heated in muffle furnace up to 500 ^oC for 1 h. The fired compacts were left to cool gradually to avoid cracking due to thermal shocks.

The produced $CuFe_2O_4/MgFe_2O_4$ core/shell compacts were reduced at 400-700 ^oC in a constant flowing hydrogen gas atmosphere (100%H2). Partial reduction (30 and 80%) was also applied for the confirmation of reduction mechanism. The course of reduction was followed up thermogravimetrically by means of a weight loss method using an automatic sensitive balance equipped with the vertical tube furnace.
The reduction extent is calculated as follows:
%reduction= [weight of O_2 removed at a given time/(weight of O_2 in $CuFe_2O_4/MgFe_2O_4$)] x 100

So the reduction extent was correlated to the removable oxygen of iron oxide and copper ferrite only because MgO cannot be reduced with hydrogen.

A gas purification system was used to obtain 99.99% purity hydrogen gas. The reduced products were identified and characterized by X-ray phase analysis technique PW 1730 with nickel filtered Cu radiation at 40 kV and 30 mA, a scanning electron microscope (SEM) (JEOL-JSM-5410), reflected light microscope (Meiji-CK3900 reflected light microscope with video camera),a vibrating sample magnetometer (VSM-9600M)and TEM (JEOL JEM-1230).

In each experiment, after the furnace was heated up to the required temperature, the core/shell compact was put inside a basket to be hanged in the balance and adjusted in the middle zone of the tube furnace in flow of purified nitrogen gas. After settling down for a few minutes, the reducing gas was passed while the N_2 gas was stopped. The reacted compact was kept in the reducing atmosphere until a constant weight was achieved and then the reduced compact was quenched in pure acetone.

3. RESULTES AND DISCSSIONS:

Pure synthesis of $CuFe_2O_4$/ $MgFe_2O_4$ core/ shell powder with nanocrystalline size of about 70 nm is confirmed through the XRD analysis. The TEM micrographs of typically $CuFe_2O_4$/$MgFe_2O_4$ core/shell nanoparticles are shown in Fig.1. It is clearly seen that $MgFe_2O_4$ coating is enwrapped on the $CuFe_2O_4$, forming core/shell structure of $CuFe_2O_4$/$MgFe_2O_4$ nanoparticles. The core $CuFe_2O_4$ is spherical and the shell of $MgFe_2O_4$ surrounded closely around the core. Also it is clearly shown that $MgFe_2O_4$ layer is uniformly formed covering all the surface of $CuFe_2O_4$ particles. Its magnetic properties was measured using VSM as shown in table 2 whereas the Hc, Br and Bs values are 40.46 Oe, 5.523 and 30 emu/g respectively

3.1. Characterization of reduced $CuFe_2O_4$/ $MgFe_2O_4$ core shell.

XRD pattern of reduced $CuFe_2O_4$/ $MgFe_2O_4$ core/ shell compacts are shown in Fig. 2. It is clearly seen that with increasing the reduction temperature from 400 to700 ^oC the peaks intensity of metallic iron, copper are increased but oxides beak intensity decreased and this confirm the progress of reduction process.

SEM examination of the reduced $CuFe_2O_4$/ $MgFe_2O_4$ core/ shell compacts is shown in Fig. 3. It is clearly seen from Fig. (3.a) that reduced compacts at 400 ^oC have irregular crystalline shape grains of different size with presence of micro-pores and absence of macro-pores. From Fig. (3.b) it shown that the micro-pores decreased and macro- type was found this is due to as the reduction temperature increase from 400 to 700 ^oC the sintering process occurred and then the particles coalesced to each other forming the dense structure with macro and micro-pores.

Fig. 4(a,b) show TEM photos of unreduced and reduced $CuFe_2O_4$/ $MgFe_2O_4$ core/ shell nanoparticles. It is obvious from Fig. (4.a) that $MgFe_2O_4$ shell layer enwrapped around $CuFe_2O_4$ core particles forming core/shell structure and the core particles seems to be with spherical shape. Figure (4.b) show the core/shell structure after the reduction process. It is clear that the core particles as dense and thick core layer (dark zone) is surrounded with shell which appears as a light zone.

The photomicrograph of $CuFe_2O_4$/ $MgFe_2O_4$ core/ shell compacts reduced at 500 and 700 ^{o}C are shown in Fig.5 It was observed that at 500 ^{o}C fine grain structure is formed with presence of many micro-pores while as the reduction temperature increased to 700 ^{o}C coalescence and sintering of the formed grain is observed with decreasing the micro-pores and increasing the macro- one

3.2. Reduction kinetics

$CuFe_2O_4$/ $MgFe_2O_4$core/shell compacts was isothermally reduced with H_2 at different temperatures from 400 to 700 ^{o}C by measuring the weight loss of the samples with the reduction time and the obtained reduction curves are shown in Fig.6. It was found that the rate of reduction increases with increasing reduction temperature that confirms with basic principle of chemical thermodynamics and kinetics as the reduction process is endothermic. The reduction was not completed at all the reduction temperatures whereas at 400-600 ^{o}C the reduction percent reached to about 87.7% while the reduction percent increase to 88.3% at 700°C. That is due to formation of very stable oxide layer of MgO which can not reduced at any degree of reduction temperature and form dense layer which hinder the penetration of hydrogen gas to deep part of the sample and so the reduction process not completed.

The kinetics of reduction of $CuFe_2O_4$/ $MgFe_2O_4$ core/ shell nanoparticles are studied over a range of temperature 400- 700 ^{o}C with hydrogen. The corresponding relationships between logarithm rate of reduction (log dr/dt) at both initial (0-25% reduction extent) and final (60- 75% reduction) stages and invest of reduction temperature with Kelvin scale (1/T) are shown in Fig. 7. Many investigators have calculated the apparent activation energy values in order to determine the rate-controlling step. The general ranges of values that have been obtained by Strangway[32] are summarized in Table 1.

To illustrate the rate controlling mechanism at both the initial and final stages of reduction, the apparent activation energy (Ea) of reduction was calculated from Arrhenius equation

$$Kr = K_o\ e^{(-Ea/RgT)}. \tag{1}$$

Where R_g = the gas constant   T = the absolute temperature
K_o = the frequency factor K_r= the rate constant
The reaction rate constant (K_r) can be derived from a rate equation of the form:

$$dr / dt\ = K_r\ P^n \tag{2}$$

P^n = pressure of the reducing gas and n= the order of reaction. From Arrhenius plots shown in Fig. 6, the activation energy for $CuFe_2O_4$/ $MgFe_2O_4$ core–shell in the initial stage was 13.9kJ/mole, while that of the final stage is 24.24 kJ/mole. These values correspond to gaseous diffusion mechanism at initial stages and combined gaseous

diffusion and interfacial chemical reaction mechanisms at the final stages of reduction.

Fig. 8 (a,b) shows the photomicrograph of partially reduced $CuFe_2O_4$/ $MgFe_2O_4$ core/shell nanoparticles to (a) 80% and (b) 30% reduction extent. It is clear that at the initial reaction stages (30%) the compact are characterized by a dense matrix of $CuFe_2O_4$/ $MgFe_2O_4$ core/ shell nanoparticles which hinders the gaseous diffusion. On the other hand, at the final stages open macro-pores is observed at the surface which facilitate the gas diffusion and so the reduction seems to be controlled by a combined effect of gas diffusion and interfacial chemical reaction.

Accordingly the grain model developed by Szekely was used for the analysis of the experimental results in this investigation. Thus, for the reduction of metal oxide with H_2 as a first order reaction, the chemical reaction control formula is as flows.

$$\Phi (X) = 1- (1 - X)^{Fg} \qquad (3)$$

Where $\Phi(x)$ is the interfacial chemical reaction control conversion factor and x is the fractional reduction. F_g is the shape factor and it was replaced by 2 for compacts in the form of long cylinders.

On the other hand the gaseous diffusion reaction control formula is

$$g(X) = X + (1 - X) \ln (1\text{-}X) \qquad (4)$$

For more evidences, the mathematical formulae for gaseous diffusion, chemical reaction and mixed control were applied. It is obvious that at the initial stages of reduction at different temperatures the relationship between g (X) and time is a straight line (Fig. 9 a) on applying the gas diffusion equation. This confirms that the gaseous diffusion is the rate controlling mechanism for sample. But at the final stages of reduction at different temperatures the relationship between Φ (X) +g (X) and time is a straight line (Fig. 9 b) on applying the mixed control formula. This confirms that the combined gaseous diffusion and interfacial chemical reaction is the rate controlling mechanisms for sample.

3.3- Magnetic properties of reduced $MgFe_2O_4$/$CuFe_2O_4$ core /shell

Magnetic measurements were done at room temperature using vibrating sample magnetometer (VSM). Fig.10 and Table 2 show the B-H hysterisis loop and the obtained magnetic values (Hc, Br, Bs) of $CuFe_2O_4$/ $MgFe_2O_4$ core/ shell reduced at different temperature. It is clearly seen that the magnetic properties affected by reduction process as in Fig. 11 which show the effect of reduction temperature on values of saturation magnetization (Bs), remnant magnetization(Br) and coercivity (Hc). It was found that as the reduction temperature increases from 400 to 700 ^{o}C there is sharp decrease in coercivity value (Hc) from 237.3 to 47.56 Oe. Also the remnant magnetization value (Br) decreased while the saturation magnetization value (Bs) increased from 122.2 emu/g at 400 ^{o}C to 161.1 emu/g at 700 ^{o}C (Table.2). The change in magnetic properties with the reduction process due to formation of metallic copper and iron layer as reduction products which have high magnetic properties more than its ferrites or oxides.

4. CONCLUSION:

Nanocrystalline $CuFe_2O_4$/$MgFe_2O_4$ core/shell (70nm) were successfully prepared by hydrothermal precipitation method. The produced nanopartecles are reduced in hydrogen flow at 400-700 ^{o}C. The formation of metallic copper and iron increased

with increasing reduction temperature. The activation energy values were calculated from Arrhenius equation and the approved mathematical formulations for the gas solid reaction were applied. The initial reaction stages are controlled by the gaseous diffusion mechanism while at the final stages the combined gaseous diffusion and interfacial chemical reaction is the controlling mechanism. Magnetic properties of the reduced $CuFe_2O_4$/ $MgFe_2O_4$ core/shell particles were studied. The core/shell magnetic properties influenced by reduction temperature whereas the saturation magnetization (Bs) increases while the coercivity (Hc) and the remnant magnetization (Br) decrease with increasing reduction temperature from 400 to 700 ^oC.

REFRENCES:

[1]   S. Sun, C.B. Murry, J. Appl. Phys. 85 (1999).
[2]   C.P. Bean, J.D. Livingston, J. Appl. Phys. 30 (1959).
[3]   R.H. Kodama, A.E. Berkowitz, E.J.Mc Niff Jr., S. Foner, J. Mater. Sci.Forum 643 (1997).
[4]   Y.Li,J.Zhao,J.Han,X.He,Mater.Res.Bull.40, 981 (2005).
[5]   Y.Li,J.Zhao,J.Han,L,Qiang,Alloys compd.373, 298 (2004).
[6]   A.J. Ruys, Y. Mai, Mater. Sci. Eng. A 265, 202_ 207 (1999).
[7]   S. Link, M.A. El-Sayed, J. Phys. Chem., B 103, 8410 (1999).
[8]   M.A. El-Sayed, Acc. Chem. Res. 34, 257 (2001).
[9]   A. Eychmuller, J. Phys. Chem., B 104, 6514 (2001).
[10] S.Y. Chang, L. Liu, S.A. Asher, J. Am. Chem. Soc. 116, 6745 (1994).
[11] J.Y. Lee, J.H. Lee, S.H. Hong, Y.K. Lee, J.Y. Choi, Adv. Mater. 15, 1655 (2003).
[12] V. Jokanovic´, A.M. Spasic´, D. Uskokovic´, J. Colloid Interface Sci. 278, 342 (2004).
[13] J.L. Yin, X.F. Qian, J. Yin, M.W. Shi, J.C Zhang, G.T. Zhou, Inorg. Chem. Commun. 6, 342 (2003).
[14] E. Matijevic, J. Appl. Chem. 64, 1703 (1992).
[15] E. Matijevic, Langmuir 10, 8 (1994).
[16] M.P. Pileni, C. Petit, J. Magn. Magn. Mater. 166, 82 (1997).
[17] P. Mulvaney, L.M. Liz-Marzan, M. Giersig, T. Ung, J. Mater. Chem. 10, 1259 (2000).
[18] F. Caruso, Adv. Mater. 13, 11 (2001).
[19] M. Paulose, C.A. Grimes, O.K. Varghese, E.C. Dickey, Appl. Phys. Lett. 81, 153 (2002).
[20] E. Matijevic, D.V. Goia, New J. Chem. 22, 1203 (1998).
[21] D.L. Peng, H. Yamada, T. Hihari, T. Uchida, K. Sumiyama, Appl. Phys. Lett. 85, 2935 (2004).
[22] E. Bonetti, L. Del Bianco, S. Signoretti, P. Tiberto, J. Appl. Phys. 89, 1806 (2001).
[23] A. A. El-Geassy, M. H. Khedr and M. I. Nasr (eds.): Proc. 5th Int. Symp. on 'Advanced materials', Islamabad, Pakistan, September 1997, AQ Khan Research Laboratories, 302.
[24] L. F. Tong: Trans. Inst. Min. Metall. C, 110, 14 (2001).
[25] S. Ebrahimi, C. Ponton and I. Harris: J. Mater. Sci., 34 , 45–52 (1999).
[26] M. H. Khedr: J. Anal. Appl. Pyrolysis, 73, 123 (2005).

[27] M. H. Khedr,A.A.Farghali,A.A.Abdel-khalek:J. Anal. Appl. Pyrolysis, 78 , 1 (2007).
[28] M.Bahgat; Mineral Processing and Extractive Metallurgy.C, 115, 4 (2006).
[29] M.H.Khedr,A.A.Farghali,A.A.Abdel-Khalek,J.Anal.App.Pyrol.78, 1 (2007).
[30] H. Zhang, Q. Qi, D.G. Evans, X. Duan, J. Solid State Chem. 177, 772 (2004).
[31] X. Duan, Q.Z. Jiao, L. Li, Chinese Patent CN 99119385.7.
[32] P.K. Strangway, M.Sc. Thesis, Terento University, (1964)

Table 1: Relationship between activation energy values and the rate controlling step.

Activation energy value Ea (kJ/mol)	Probable rate controlling step
8–16 29–42 60–67 >90	Gas diffusion Combined gas diffusion and interfacial chemical reaction Interfacial chemical reaction Solid-state diffusion

Table 2: Magnetic properties of reduced samples of $CuFe_2O_4$/$MgFe_2O_4$ core/shell nanoparticles.

sample	Bs (emu/g)	Br(emu/g)	Hc (Oe)
Unreduced $CuFe_2O_4$/$MgFe_2O_4$	30	5.523	40.46
$CuFe_2O_4$/$MgFe_2O_4$ Reduced at 400 ^{o}C	122.2	10.53	237.3
$CuFe_2O_4$/$MgFe_2O_4$ Reduced at 500 ^{o}C	122.4	3.521	117.7
$CuFe_2O_4$/$MgFe_2O_4$ Reduced at 600 ^{o}C	155.3	3.582	85.12
$CuFe_2O_4$/$MgFe_2O_4$ Reduced at 700 ^{o}C	161.1	1.196	47.56
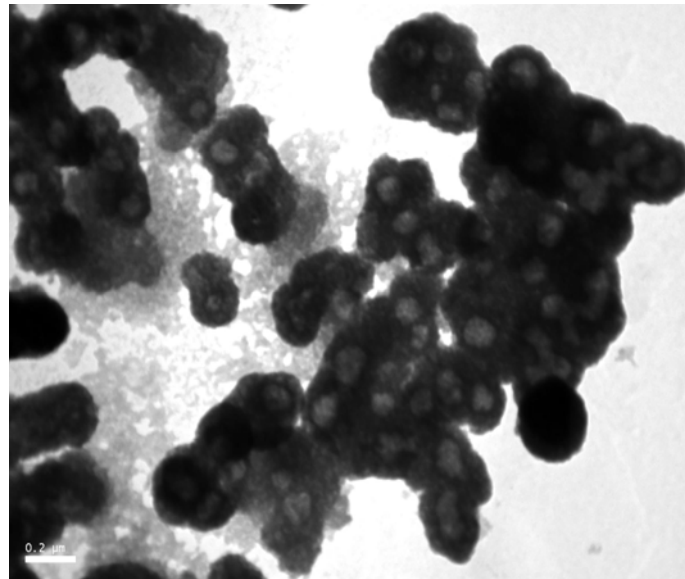
Fig. 1:TEM of CuFe2O4/MgFe2O4core/shell nanoparticles.
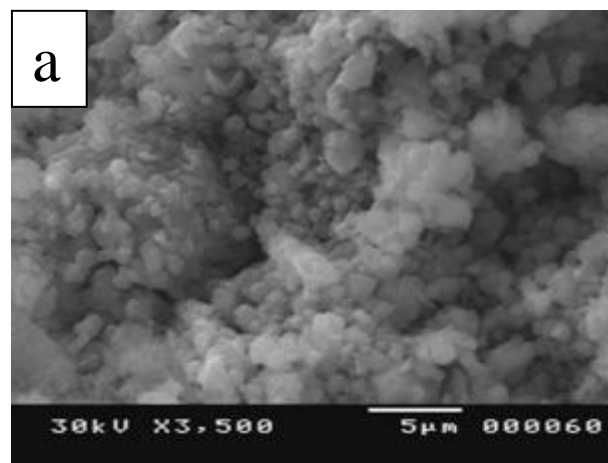
Fig.2: XRD patterns for CuFe2O4/ MgFe2O4 core/shell reduced at different temperature.
(1)Iron, (2)Copper, (3)Magnesium oxide (4)Magnesium iron oxide and (5)Copper oxide.
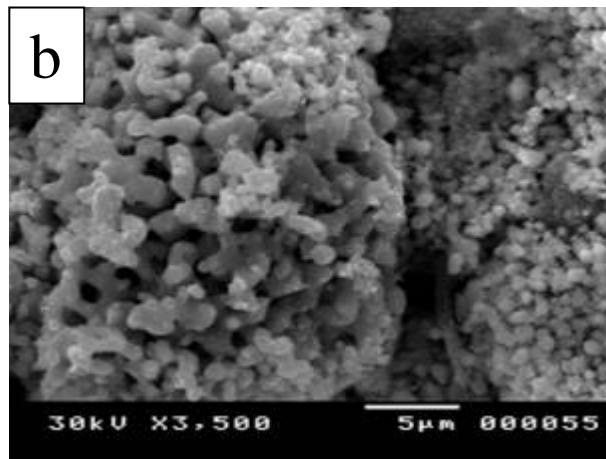
Fig. 3: SEM of CuFe2O4/ MgFe2O4 core shell reduced at
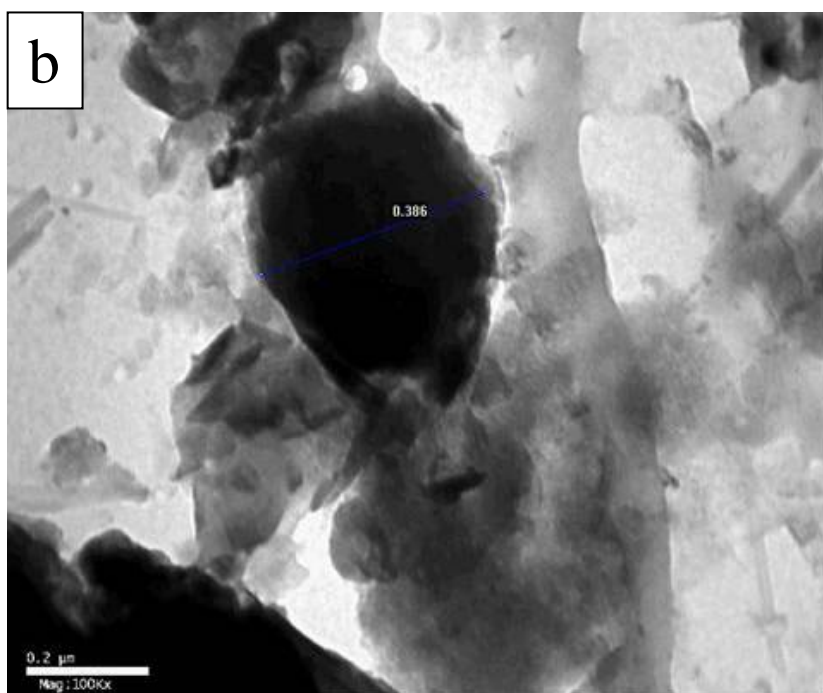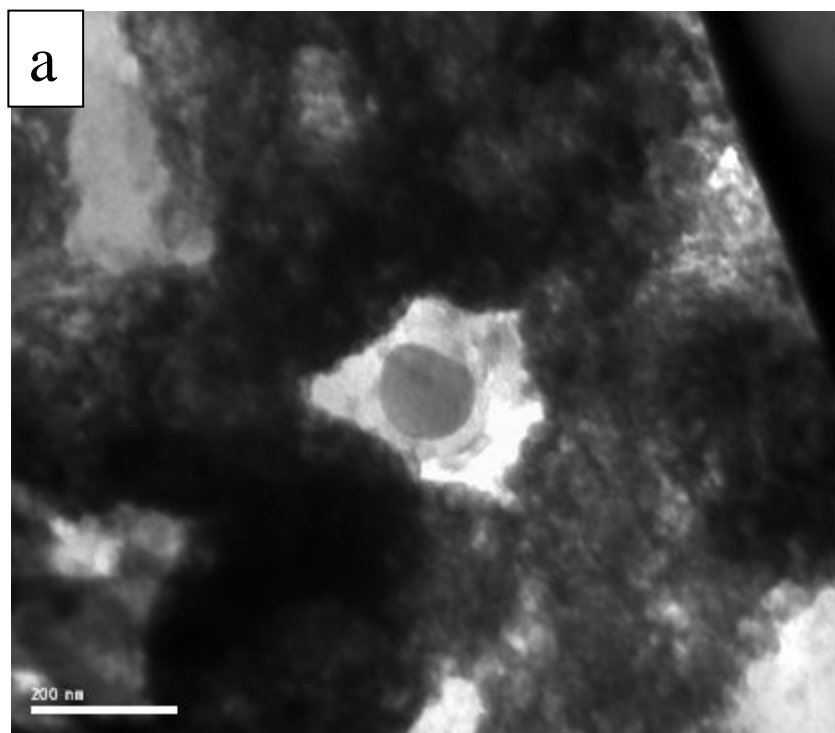(a) 400 oC (b) 700 oC.

Fig. 4: TEM photos of (a) unreduced CuFe2O4/MgFe2O4 core shell nanoparticles (x 120K), (b) reduced CuFe2O4/MgFe2O4 core shell nanoparticles at 700 oC (x 100K).
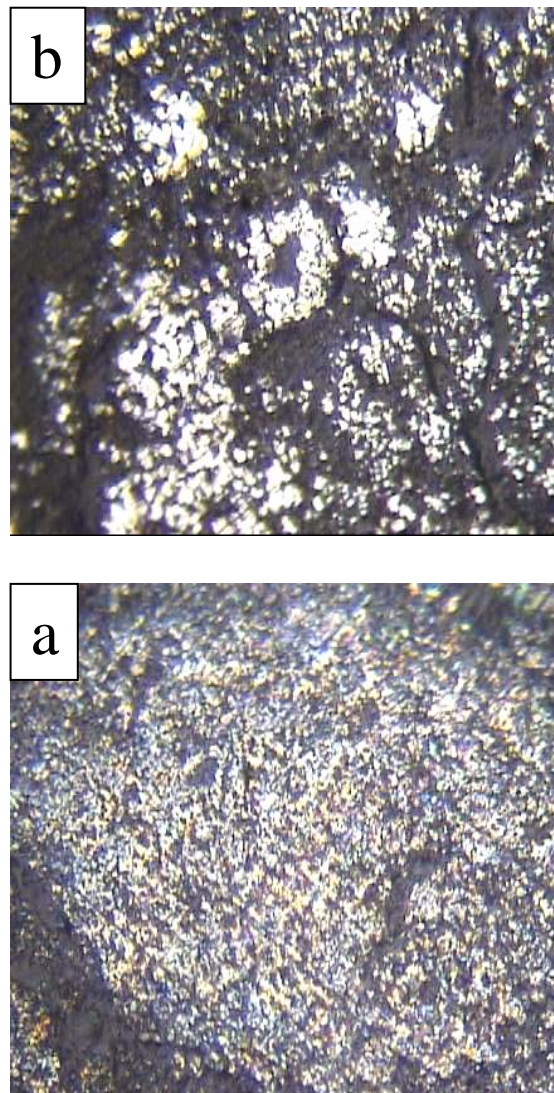
Fig. 5: Photomicrographs of reduced CuFe2O4/MgFe2O4 core shell nanoparticles at different temperature (a) 500 oC (b) 700 oC (x400)
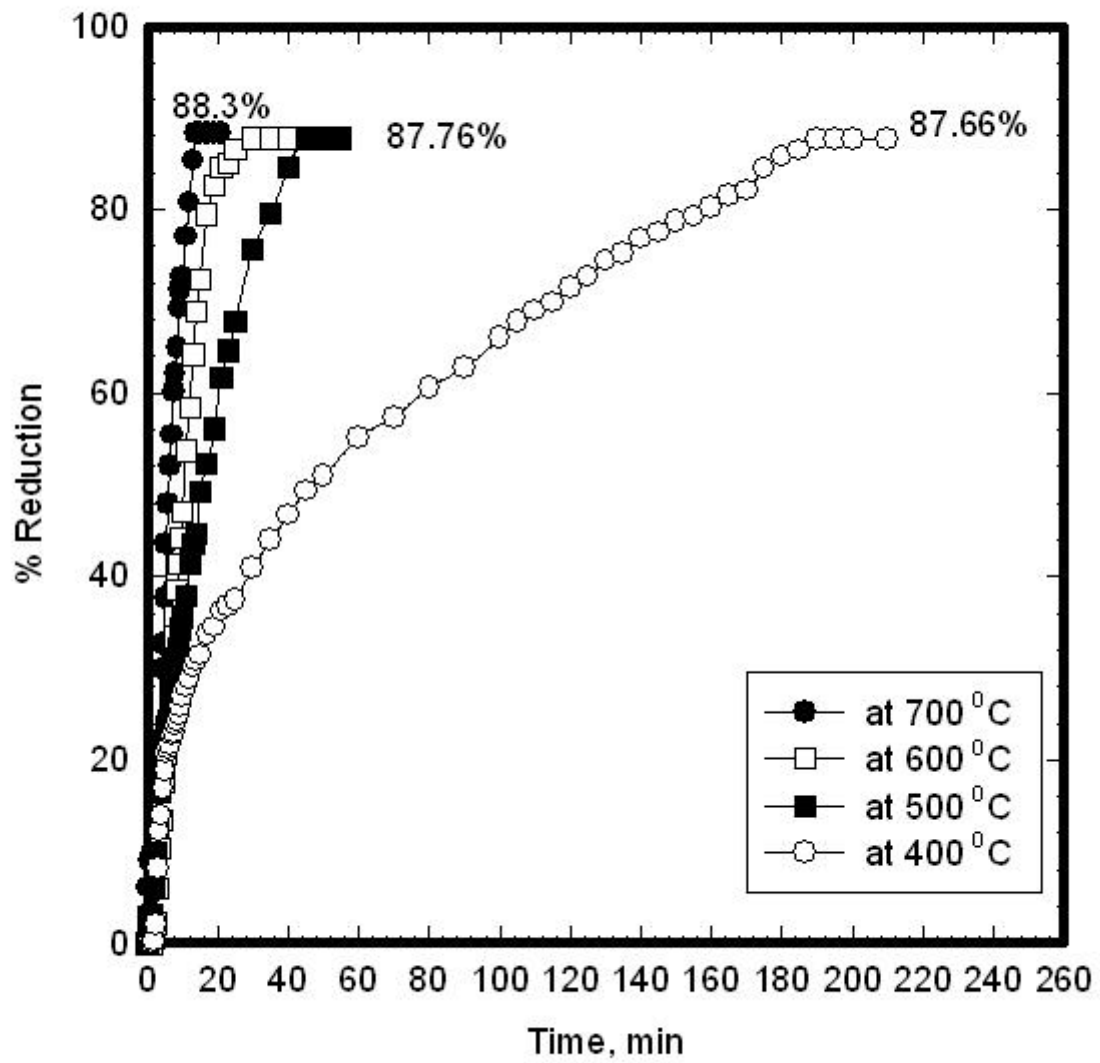
Fig. 6: Reduction curves of CuFe2O4/MgFe2O4 core/shell at different temperature.
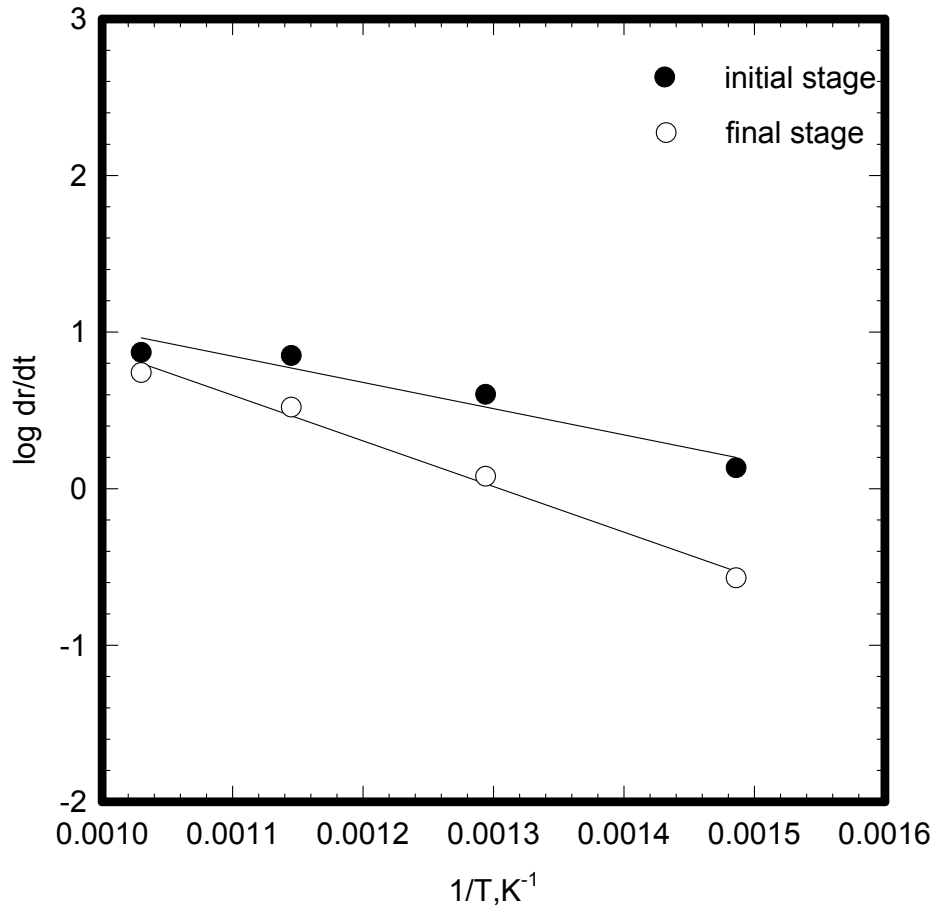
Fig. 7. Arrhenius plots for CuFe2O4/MgFe2O4 core/shell reduction at the initial and final stages.
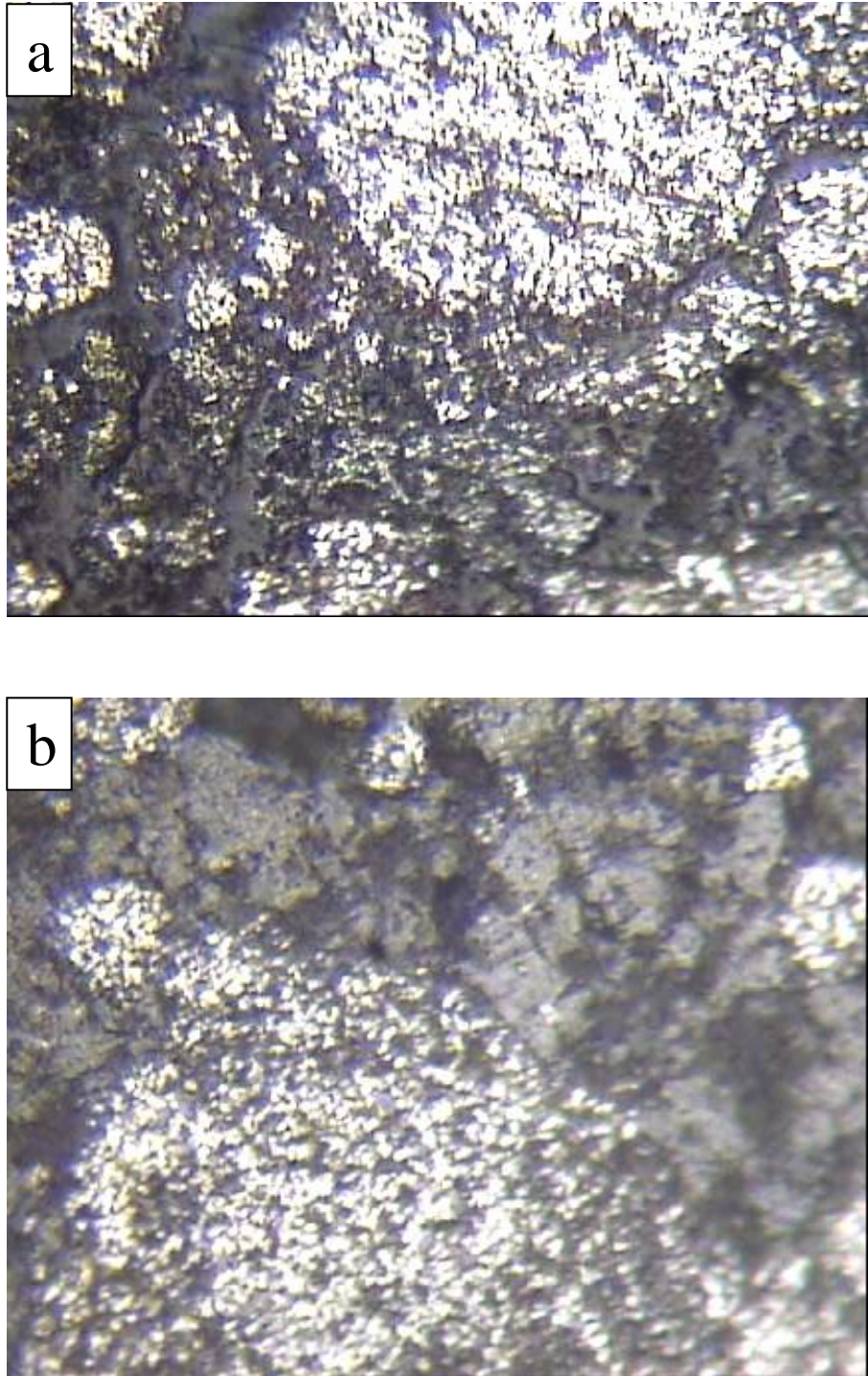
Fig. 8 : Photomicrograph of CuFe2O4/MgFe2O4 core/shell sample partially reduced at 600 oC to(a) 80% (b)30%   (x 400).
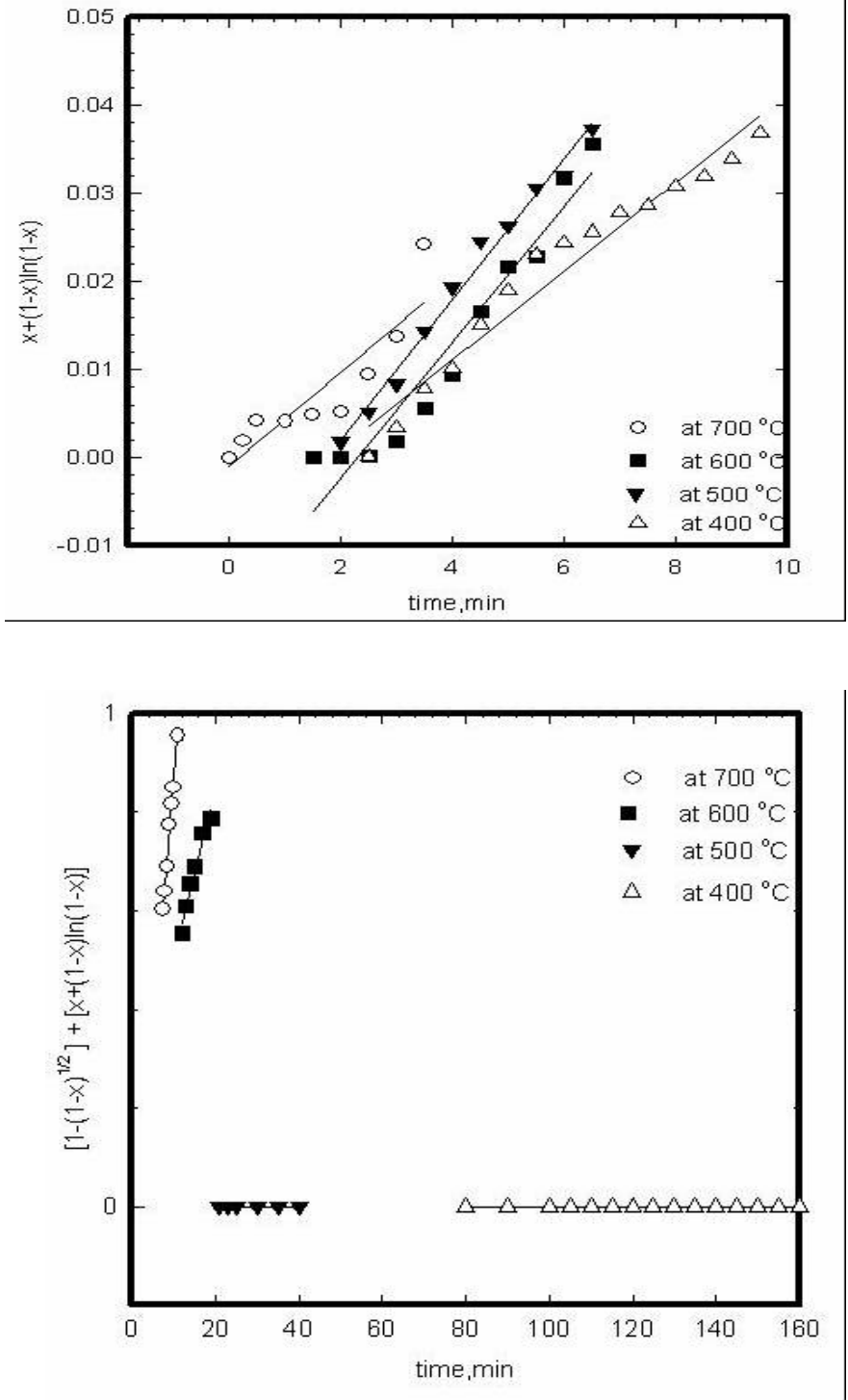
Fig. 9. (a) Application of gaseous diffusion control equation at the initial stages (b) Application of the combined chemical reaction and gaseous diffusion control equations at the final stages for CuFe2O4/MgFe2O4core/shell reduction at 400-700 oC .
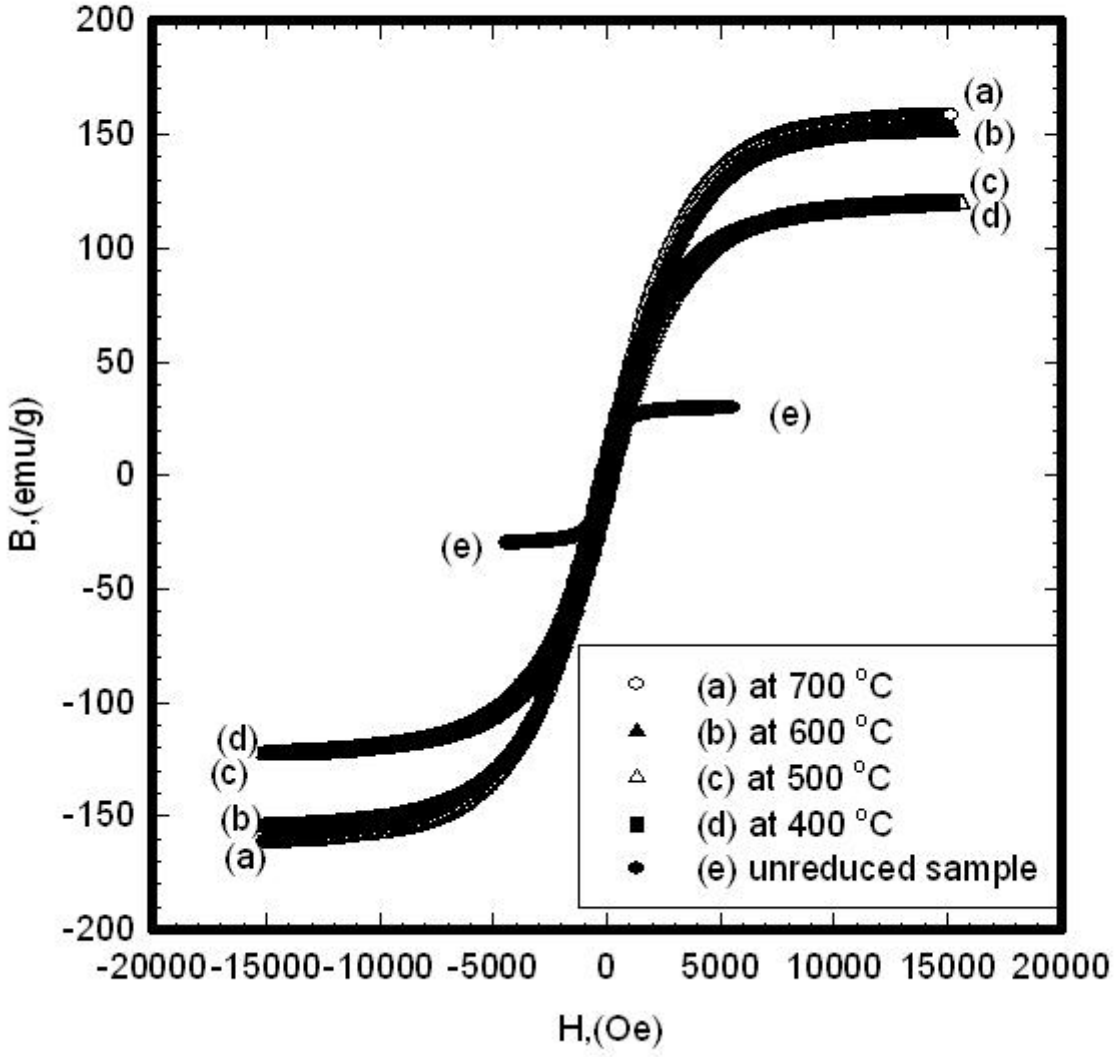
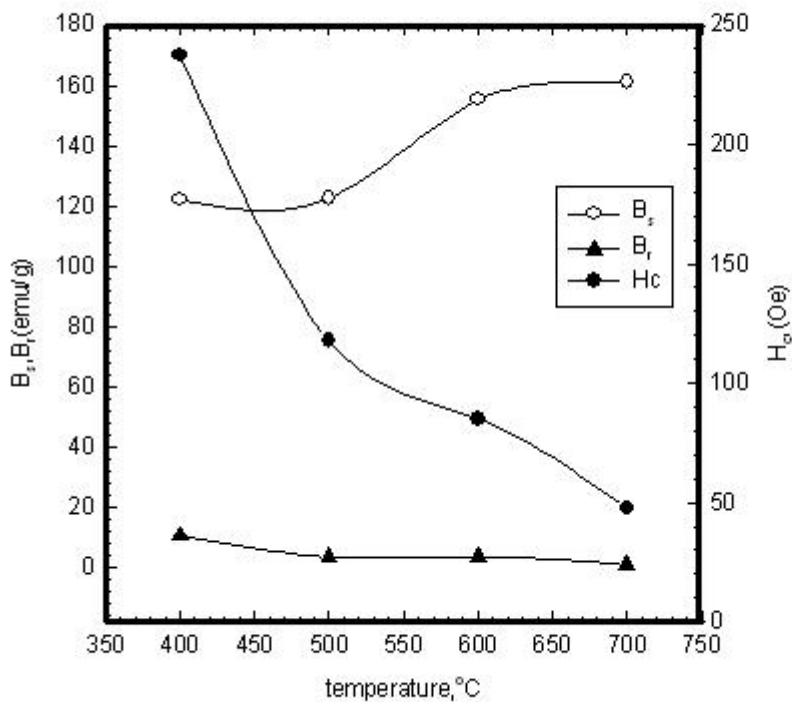Fig. 10: B-H hysterisis loop of CuFe2O4/MgFe2O4 core/shell reduced at different temperature.

Fig. 11: Relation between B_s, B_r, H_c and reduction temperature for CuFe$_2$O$_4$/MgFe$_2$O$_4$ core/shell nanoparticles.